TITLE: HER3 is an Actionable Target in Advanced Prostate Cancer.

Veronica Gil[1, #], Susana Miranda[1, #], Ruth Riisnaes[1,2], Bora Gurel[1], Maria Antonietta D'Ambrosio[3], Alessandro Vasciaveo[4], Mateus Crespo[1,2], Ana Ferreira[1], Daniela Brina[3], Martina Troiani[3], Adam Sharp[1,2], Beshara Sheehan[1], Rossitza Christova[1], George Seed[1], Ines Figueiredo[1], Maryou Lambros[1], David Dolling[1], Jan Relowski[1], Abdullah Alajati[3], Matthew Clarke[1], Rita Pereira[1], Penny Flohr[1], Gemma Fowler[1], Gunther Boysen[1], Semini Sumanasuriya[1,2], Diletta Bianchini[1,2], Pasquale Rescigno[1,2], Caterina Aversa[1,2], Nina Tunariu[1,2], Christina Guo[1,2], Alec Paschalis[1,2], Claudia Bertan[1], Lorenzo Buroni[1], Jian Ning[1], Suzanne Carreira[1], Paul Workman[1], Amanda Swain[1], Andrea Califano[4], Michael M. Shen[4], Andrea Alimonti[3], Antje Neeb[1], PCF/SU2C International Prostate Cancer Dream Team, Jonathan Welti[1], Wei Yuan[1], Johann de Bono[1,2] *.

[#] These authors contributed equally to this work

Affiliations:

1. The Institute of Cancer Research, London, UK.

2. The Royal Marsden Hospital, London, UK.

3. Institute of Oncology Research, Università della Svizzera Italiana, Bellinzona, Switzerland.

4. Columbia University College of Physicians and Surgeons, New York, USA.

RUNNING TITLE: HER3 is an Actionable Target in Advanced Prostate Cancer.

Corresponding author and lead contact:

Professor Johann de Bono

Regius Professor of Experimental Cancer Medicine

The Institute of Cancer Research

15 Cotswold Road

London

1

UK SM2 5NG

T +44 (0) 208 722 4029

F +44 (0) 208 642 7979

E johann.de-bono@icr.ac.uk

CONFLICT OF INTEREST STATEMENT

J. d. B. has served as an occasional consultant/advisory board member for Astellas, AstraZeneca, Bayer, Daiichi Sankyo, Genentech-Roche, Genmab, GSK, Janssen Oncology, MSD, Merck-Serono, Orion Pharma, Pfizer, Sanofi-Aventis.

P. W. is a nonexecutive director of Storm Therapeutics; is Executive Director of the non-profit Chemical Probes Portal; holds ownership interest in Storm Therapeutics, Chroma Therapeutics and Nextechinvest; is a consultant/advisory board member for Astex Therapeutics, CV6 Therapeutics, Black Diamond Therapeutics, Vividion Therapeutics, Nuvectis Pharma and Nextechinvest; has received commercial research grants from Vernalis, Astex Pharmaceuticals, Merck and Sixth Element; and is former Chief Executive of The Institute of Cancer Research, which has a range of interactions with industry.

A.S. has received travel support from Sanofi and Roche-Genentech, and speakers' honorarium from Astellas Pharma.

G.B. has now become an employee of Astellas Pharmaceuticals.

P.R. served on the Advisory Board of MSD and Astra Zeneca Italy.

A.C. is founder, equity holder, and consultant of DarwinHealth Inc., a company that has licensed some of the algorithms used in this manuscript from Columbia University. Columbia University is also an equity holder in DarwinHealth Inc.

The Institute of Cancer Research has a commercial interest in abiraterone.

The other authors declare no conflicts of interest.

ABSTRACT

It has been recognized for decades that ERBB signaling is important in prostate cancer (PC), but targeting ERBB receptors as a therapeutic strategy for prostate cancer has been ineffective clinically.

2

However, we show here that membranous HER3 protein is commonly highly expressed in lethal PC, associating with reduced time to castration resistance (CR) and survival. Multiplex immunofluorescence indicated that the HER3 ligand NRG1 is detectable primarily in tumor-infiltrating myelomonocytic cells in human PC; this observation was confirmed using single cell RNA-seq of human PC biopsies and murine transgenic PC models. In CRPC patient-derived xenograft organoids (PDX-O) with high HER3 expression as well as mouse PC organoids, recombinant NRG1 enhanced proliferation and survival. Supernatant from murine bone marrow-derived macrophages and myeloid-derived suppressor cells promoted murine PC organoid growth in vitro, which could be reversed by a neutralizing anti-NRG1 antibody and ERBB inhibition. Targeting HER3, especially with the HER3 directed antibody-drug conjugate U3-1402, exhibited antitumor activity against HER3-expressing PC. Overall, this data indicates that HER3 is commonly overexpressed in lethal PC and can be activated by NRG1 secreted by myelomonocytic cells in the tumor microenvironment, supporting HER3-targeted therapeutic strategies for treating HER3-expressing advanced CRPC.

SIGNIFICANCE: HER3 is an actionable target in prostate cancer, especially with anti-HER3 immunoconjugates, and targeting HER3 warrants clinical evaluation in prospective trials.

3

INTRODUCTION

Prostate cancer (PC) remains one of the commonest male malignancies, and a leading cause of male cancer mortality with increasing global incidence (1). Genomic studies have demonstrated that PC is a highly heterogeneous group of diseases, most of which are addicted to oncogenic androgen receptor (AR) signaling (2,3). PCs usually initially respond to androgen-deprivation therapy (ADT), but, if not cured by radical local treatment, clinical progression to metastatic castration-resistant PC (mCRPC) invariably occurs. Persistent AR signaling from constitutively active AR splice variant expression (4), AR aberrations, as well as AR enhancer activity and AR co-factor function contribute to treatment resistance (5). Other pathways commonly aberrant in PC include PI3K/AKT and MEK/ERK signaling, loss of RB1 function, cell cycle aberrations, and hijacked WNT signaling (3).

For decades, it has been recognized that ERBB signaling is implicated in CRPC (6), but clinical trials of ERBB targeting drugs including studies of pertuzumab targeting HER2/HER3 heterodimerization, and the small molecule ERBB inhibitor afatinib, in combination with ADT, failed to demonstrate antitumor activity (7,8). Unlike breast cancer (9) genomic aberrations in ERBB/HER genes are uncommon in PC (10). Consequently, the clinical evaluation of ERBB/HER receptor targeting for PC has been largely abandoned, despite the plethora of anticancer drugs targeting these receptors for the treatment of other cancers, including immunoconjugates targeting HER2 and HER3 (11-13). We elected to re-investigate ERBB receptors in endocrine treatment-resistant lethal PC, hypothesizing that targeting ERBB receptors merits further evaluation in mCRPC.

MATERIALS AND METHODS

Patient sample collection. Patients were identified from a population of men with mCRPC treated at the Royal Marsden NHS Foundation Trust. All patients had given written informed consent and were enrolled in institutional protocols approved by the Royal Marsden NHS Hospital (London, UK) ethics review committee (reference no. 04/Q0801/60). Human biological samples were sourced ethically, and their research use was in accord with the terms of the informed consent provided. We analyzed 88 patients with sufficient formalin-fixed, paraffin embedded (FFPE) diagnostic (archival) castration-sensitive PC (CSPC) biopsies; 51 of these 88 patients had sufficient matching FFPE mCRPC biopsies (*Supplementary Figure 1 and Supplementary Table 1*). All CSPC biopsies demonstrated adenocarcinoma and were from either prostate needle biopsy (n=72), transurethral resection of the prostate (TURP; n=6), prostatectomy (n=4) or alternative sites (n=6). CRPC tissue was obtained from metastatic biopsies of bone (n=25), lymph node (n=19), soft tissue (n=3), liver (n=2) and TURP (n=2). All tissue blocks were freshly sectioned and only considered for immunohistochemistry (IHC) analyses if adequate material was present (≥50 tumor cells;). Demographic and clinical data for each

4

patient were retrospectively collected independently by A.S. and S.S. from the hospital electronic patient record system.

Immunohistochemistry. Tissue blocks were sectioned and only considered for analyses if adequate material was present. Protein expression was determined via IHC on 3-4 μm thick FFPE sections and assessed by a PC pathologist (BG) blinded to the clinical data. All cases were subsequently imaged at high resolution and scored with image analysis software. More details on the immunohistochemistry assays used are available in the ***Supplementary Materials and Methods and Supplementary Table 2***.

Multicolor Immunofluorescence panel for NRG1, CD11b, CD68 and DAPI. Multiplex tissue IF staining for NRG1, CD11b and CD68 was performed on the Bond RX automated staining platform (Leica Biosystems) with the Opal 7-Colour Automation IHC Kit (NEL821001KT, Akoya Biosciences) according to the manufacturer's instructions. IF signals for NRG1, CD11b and CD68 were visualized using TSA dyes 570, 520 and 650 respectively, and counterstained with spectral DAPI. After staining, slides were scanned using the VS200 Microscope (Olympus) and quantification of immune cell densities expressing NRG1 was achieved with Halo v3.0 software (Indica Labs). More details on the IF assay is available in ***Supplementary Table 2***.

Genomic characterization and mutation analysis. Patient tumor samples were analyzed as previously described (14). Briefly FFPE DNA samples were extracted with the FFPE tissue DNA kit (Qiagen), libraries were constructed for targeted sequencing using a 113 genes custom designed panel (Generead V2, Qiagen) and then sequenced on an Illumina MiSeq with a 300 cycles V2 reagent (2x150). FastQ files were generated and analyzed through the Qiagen Web portal: https://ngsdataanalysis.qiagen.com. Where mutation data was available, for either CSPC or CRPC (n=41), patients were grouped into DDR Yes/No based on the evidence of DNA Damage Repair alterations. Association with membranous HER3 (mHER3) OD was analyzed using Mann-Whitney, non-parametric, two-tailed test.

RNA-sequencing. Cell line, Patient Derived Xenograft (PDX), and Organoid RNA quality was analyzed using Agilent RNA ScreenTape assay (Agilent). 500 ng of total RNA from each cell line and PDX sample and 10 ng of total RNA from each organoid sample was used for library preparation using the NEBNext rRNA depletion kit followed by NEBNext Ulta II directional RNA assay kit as per manufacturers protocol (New England Biolabs). Library quality was confirmed using the Agilent High sensitivity D1000 ScreenTape Assay (Agilent). The libraries were quantified and normalized by qPCR using Generead Library Quant Kit (Qiagen). Library clustering and sequencing were performed on the Illumina NovaSeq 6000. The libraries were run across two lanes of an Illumina NovaSeq S2 flowcell using 150 base pair pair-end v1 Kit and eight base pair dual indexes. Base-calling and quality scoring were performed using Real-Time Analysis (version v3.4.4) and FASTQ file generation and de-multiplexing using Illumina bcl2fastq2 (version 2.20).

5

Development of lethal prostate cancer PDX CP142.

CP142 PDX model was developed as previously described for CP50 ([15,16](#)). Briefly, a metastatic lymph node biopsy from a patient with CRPC was divided and implanted subcutaneously into an intact non-obese diabetic (NOD) scid gamma (NSG) (NOD.Cg-*Prkdcscid Il2rgtm1WjI*/SzJ) between 7-8 weeks of age male mice (termed CP142). Tumor growth was observed 6 months after implantation. Passaging of tumors was performed by implanting tumor fragments of 3 x 3 x 3 mm subcutaneously into male NSG mice. To generate castrate (C) lines termed CP142C, tumors that had been passaged 4 times were castrated when they reached 300 to 400 mm^3 and were harvested when they reached a size of around 1200 mm^3. Subsequent passages were done in castrated mice. All experimental protocols were monitored and approved by The Institute of Cancer Research Animal Welfare and Ethical Review Body, in compliance with guidelines specified by the UK Home Office Animals (Scientific Procedures) Act 1986 and the United Kingdom National Cancer Research Institute guidelines for the welfare of animals in cancer research ([17](#)).

Organoid culture (PDOs). Fresh PDX tumors from mCRPC patients were collected and immediately placed into biopsy transport media with additional ROCK inhibitor Y27632 at 10 μM (S1049, Selleckchem). Tissue was mechanically dissociated to generate a single cell suspension. Cells were embedded into extracellular matrix containing mitogens and niche factors to generate organoids as previously described ([18](#)) (***Supplementary Materials and Methods and Supplementary Tables 3***).

Western blotting. Cells and PDX-O were lysed with RIPA buffer (Pierce) supplemented with protease inhibitor cocktail (Roche) and and PhosStop phosphatase inhibitor mix (Roche). PDX lysate was obtained by mechanical homogenization, reconstituted in RIPA buffer. Protein extracts (20μg) were separated on 4-12% NuPAGE® Bis-Tris gel (Invitrogen) by electrophoresis and subsequently transferred onto Immobilon-P™ PVDF membranes of 0.45μm pore size (Millipore). Chemiluminescence was detected on the Chemidoc™ Touch imaging system (Bio-Rad). Detailed antibodies in ***Supplementary Table 3.***

RNA and DNA extraction. Organoids were collected using harvesting solution (3700-100-01, Cultrex Amsbio) into conical Eppendorf tubes and incubated on ice for 30min to remove extracellular matrix then washed 1x with cold sterile PBS and pelleted by cold spin. Extraction for RNA and DNA was performed using the *Quick* prep kits (Zymo Research) following manufacturers protocols. PDX RNA was obtained by mechanical homogenization, reconstituted in RLT and then extraction was performed using the RNeasy plus kit following manufacturers protocol (Qiagen).

Single-cell analysis of PC patient samples. Single-cell RNA-seq profiles from 13 prostate tumor samples were downloaded as UMI matrix from GEO:GSE141445 ([19](#)). The UMI matrix was processed using scanpy (v1.7.1) ([20](#)) and Python (v3.8.4). Quality control was performed retaining

6

cells with more than 500 detected genes and with at least 1,500 unique reads. Cells with more than 10,000 detected genes were discarded as potentially cell doublets. Cells with genes detected only in less than 5 cells were also discarded. Only cells with mitochondrial gene content below 10% of total reads were retained. After quality control, 30,329 cells were retained. Next, we transformed the data using 1e6 as scaling factor, and log-normalized the resulting counts per million matrix. Data was scaled and centered for downstream analysis. Principal Component Analysis (PCA) and K-Nearest Neighbor (KNN) analyses were performed using n=15 neighbors, n=6 Principal Components (PCs) and euclidean distance metric. We used the elbow method to determine the number of PCs to use for downstream analysis. To identify clusters of cells that recapitulate cell populations independently from the patient sample from which were collected, we performed batch-balanced KNN analysis using BBKNN (v1.4.1) ([21]). We performed clustering analysis using the Leiden algorithm with resolution parameter set to 0.15 ([22]). This analysis identified 8 clusters that were used for downstream analysis. Next, the log-transformed matrix was used as input for the SingleR algorithm to perform single-cell level automated cell type annotation ([23]) in the R environment (v4.0.4). We used the Blueprint and ENCODE reference datasets, that consists of bulk RNA-seq data for pure stroma and immune cells generated by Blueprint ([24]) and ENCODE projects ([25]). For each cluster we assigned a label based on the most common cell type inferred from the SingleR analysis, using a majority voting system. SingleR inference was not tuned, and only low granularity cell type assignments were processed. Cell type labelling was manually refined based on differentially expressed genes computed using the Wilcoxon test, by comparing each cluster against all the others. We used the Bonferroni method to correct for multiple hypothesis testing. We used the Uniform Manifold Approximation and Projection (UMAP) to display cells on a two-dimensional space ([26],[27]).

Conditioned media collection from BM derived-MDSCs and Macrophages: Bone marrow derived cells (BMDC) were collected and flushed from long bones of C57BL/6N mice and cultured with specific cytokines. For macrophage differentiation, BMDC were cultured in non-adherent cell culture 6-well plates (4×10^6 cells/well) in IMDM supplemented with 10% heat-inactivated-FCS, 5% Penicillin/streptomycin (P/S) and 10 ng/mL M-CSF for 4-days ([28]). At day 4, 70% of the media was removed and organoid media was freshly added ([18]). After 48-hours, macrophage conditioned media (M-CM) was collected and filtered with a 0.22 μm filter. For myeloid derived suppressor cells (MDSCs), BMDC were cultured in 6-well culture plates at 1.5×10^6 cells/well in RPMI supplemented with 10% heat-inactivated-FCS, 5% P/S and 40 ng/mL of IL-6 and GM-CSF for 4-days ([29]). Differentiated BM cells were then collected and re-seeded at 3×10^6 cells/well in 70% of organoid media (without additional rhEGF) and 30% of original media. After 48-hours, the MDSC-CM was collected and filtered with a 0.22 μm cell strainer. The CMs were used to treat mouse prostate cancer organoids. Organoids were obtained from the prostates of 10-week old *Pten$^{-/-}$;Trp53$^{-/-}$* transgenic mice as previously described ([18]). Mouse PC organoids were digested with TrypLE (12605-010, Life

7

Technologies) to obtain single cell suspensions seeded in 96-well plates (1000 cells/well). After 2-3 days, organoids were treated with rhNRG1 at 100 ng/mL (100-03, Peprotech) alone or in combination with M-CM or MDSC-CM (without r-hEGF). After 5-days, proliferation was assessed using CellTiter-Glo 3D Cell Viability Assay (G9681, Promega) according to manufacturer's instructions.

In vivo cell growth inhibitory activity. Tumor-bearing mice were intravenously administered U3-1402 (10mg/Kg), IgG-ADC (MAAA-9289, 10mg/Kg), anti-HER3 antibody Patritumab (U3-1287, 10mg/Kg) and 10mM acetate buffer-5% sorbitol-pH 5.5 as vehicle control for a total 5 weekly doses (CP50). A subgroup of mice (n=6) treated with U3-1402 were monitored for tumor regrowth for up-to-60-days. Total weekly dosing for CP142 model was three. Tumor growth measurements were taken every 2-3 days and grouped by 5-day intervals. Experiment was terminated and samples were collected 7-days after the last dose. Each point represents the mean tumor volume and SEM (n = 6-10) per arm of the study. Statistical significance was analyzed using ANOVA with Dunnett's multiple comparisons.

Statistical analyses. HER2 and HER3 protein levels were reported as median values with interquartile ranges (IQR). For paired, same patient, CSPC and CRPC expression studies the Wilcoxon matched-pair rank test was used to compare differences in protein (mHER3 and mHER2) expression levels. Time to CRPC was defined as the time from diagnosis (date of diagnostic biopsy unless clinical diagnosis was recorded as >1 month prior to biopsy) to documented progression (radiological, PSA or change of treatment) on luteinising hormone-releasing hormone (LHRH) agonist alone or with anti-androgen if started before/or with LHRH agonist. Overall survival was defined as time from diagnosis to date of death (73 patients) or last follow up/contact (15 patients; data cut-off 07/02/2019). Patient's outcomes were compared by mHER3 OD at diagnosis (< or ≥ median OD), median overall survival and time to CRPC were estimated using the Kaplan-Meier method. Statistical analysis of *in vivo* and *in vitro* studies was performed using ANOVA for all arms of the study with Dunnett's multiple comparisons correction test and Sidak or Bonferroni corrections where applicable. All analyses were conducted, and graphs generated, using GraphPad Prism v7.

Bioinformatic analyses. Data from CRPC transcriptomes generated by the International Stand Up To Cancer/Prostate Cancer Foundation (SU2C/PCF) Prostate Cancer Dream Team were reanalyzed (3). SU2C transcriptome and cell line transcriptome reads were aligned to the human reference genome (GRCh37/hg19) using TopHat2 (version 2.0.7).
PDX transcriptome reads were aligned to human hg19 and mouse mm9 genome. Gene expression, fragments per kilobase of transcript per million mapped reads (FPKM), was calculated using Cufflinks (30).

RESULTS

8

HER3 is highly expressed in lethal prostate cancer and has clinical relevance

We first analyzed the transcriptomes of 159 mCRPC clinical biopsies acquired by the PCF/SU2C International Prostate Cancer Dream Team ([2],[3]) and found that *ERBB2* and *ERBB3* mRNA were highly overexpressed (top 25% quartile), unlike *EGFR* and *ERBB4 (Figure 1A);* we also observed a highly significant positive correlation (Spearman $p=8.4 \times 10^{-9}$) between *ERBB2* and *ERBB3* mRNA expression *(Figure 1B).* The HER2 protein has no known ligand, while HER3 is activated by its high affinity ligands NRG1 and NRG2 but generates little signaling without heterodimerization; NRG1 and NRG2 were expressed at very low levels in mCRPC biopsy RNAseq *(Supplementary Figure 1A).* To further explore these findings, we optimized immunohistochemical assays for HER2 and HER3 *(Supplementary Figure 1B)* and established a digital, quantitative, method to assess immunohistochemical HER2 and HER3 membranous (mHER2 and mHER3) staining by automated optical density (OD) assessment utilizing Halo^{TM} (Indica Labs) image analysis software. We demonstrated a robust correlation between a visually generated score, by a pathologist, and automated optical density scores from these tumor samples by automated OD assessment (Spearman r=0.86; p<0.0001; *Supplementary Figure 1C*). Using these assays, we next evaluated HER2 and HER3 protein expression in metastatic PC samples (*Figure 1C)*, studying treatment-naïve/ CSPC biopsies from 88 men; for 51 of these men, we had matching, same-patient, mCRPC biopsies *(Supplementary Figure 1D and Supplementary Table 1*). Membranous HER2 and HER3 proteins were detectable in both CSPC and mCRPC biopsies, with HER3 being very highly expressed in many tumors (*Figure 1C*). There was a significant correlation observed between HER2 and HER3 IHC expression at CSPC (*Supplementary Figure 1E*).

To investigate the clinical significance of mHER3 expression in PC, we next evaluated these CSPC biopsies from 88 men; the median OD for mHER3 expression at diagnosis in 88 CSPC biopsies was 2958.0 (IQR 1643.0-5170.0); PC with high mHER3 expression (> median OD; n=44) had a significantly shorter median time to CRPC (20.3 vs 14.2 months; HR 0.61; 95% CI 0.40-0.94; p=0.016) and worse overall survival (OS) (79.0 vs 48.8 months; HR 0.63; 95% CI 0.39-1.00; p=0.04) compared to CSPC with low mHER3 ($\leq$ median; n=44) *(Figure 1D-E).* mHER2 staining did not associate with outcome. Overall, these data suggest that HER3 expression in lethal PC has clinical relevance.

We also studied matched, same-patient, biopsies (n=51) for mHER2 expression; mHER2 protein expression was low but increased from treatment-naïve CSPC (median OD; interquartile range (IQR): OD 155.5; 62.2-307.6) to mCRPC (median OD; IQR: OD 404.4; 46.4-596.9). mHER3 expression was very high in both CSPC and mCRPC biopsies, but surprisingly decreased slightly although remaining high (p=0.007) from CSPC (median and IQR in CSPC: OD 2373.0; 879.9-5225.0) to mCRPC (median and IQR in mCRPC: OD 980.4; 259.7-2540.0) (*Supplementary Figure 1F*). This may be

9

explained by the timing of our mCRPC biopsy acquisition, these being taken after discontinuation of the next generation hormonal agents abiraterone and enzalutamide in the face of a rising PSA; previous reports indicate that increased AR signaling upregulates the E3 ubiquitin ligase RNF41/nrdp1 (neuregulin receptor degradation protein-1) that decreases HER3 protein levels (31).

Interestingly, treatment-naïve diagnostic biopsy/CSPC mHER3 expression associated with Ki67 expression in 74 available samples (*Supplementary Figure 1G and Supplementary Table 2).* IHC analysis in diagnostic biopsies showed no correlation between mHER3 OD and ERG expression (by IHC), PTEN loss (by IHC; H-score <10), or DDR defects detected by next generation sequencing in both CSPC and CRPC samples (*Supplementary Figure 1H).*

HER2 and HER3 expression was detected at a much lower level in benign prostatic samples; in these, HER2 protein expression was weak, with incomplete membranous staining in a small number of glands and a very low median mHER2 OD of 8.3 (IQR 2.7-38.4, n=6). Cytoplasmic HER2 staining was likewise very weak. Similarly, mHER3 protein in benign prostatic glands was either low or absent. The median mHER3 OD in benign glands was 179.8 (IQR 0.5-280.2, n=5), with accompanying weak cytoplasmic staining (*Supplementary Figure 1I*). Overall, these data suggested that HER2 and HER3 play a clinically important role in PC biology (32,33) .

HER3 is highly expressed in CRPC patient-derived xenografts

We have previously described CP50, a PDX generated from a metastatic CRPC biopsy with chromosome 8 gain (MYC locus), AKT and AR amplification and ATM loss (15,16). The CP142 PDX was developed from the lymph node biopsy of a patient with low PSA and a PC with neuroendocrine (NE) differentiation progressing on androgen deprivation therapy, who proceeded to platinum-based chemotherapy after this biopsy *(Supplementary Figure 2A).* Whole-exome sequencing of the lymph node biopsy of origin and the CP142 PDX *(Supplementary Figure 2B)* revealed a common and deleterious TP53 Y220C mutation with immunohistochemical studies revealing RB1 loss and synaptophysin positivity *(Supplementary Figure 2C).* After establishing CP142 in intact mice, a subset of this PDX was developed and maintained exclusively in castrate mice and designated CP142C *(Supplementary Figure 2A).* We studied HER3 expression and signaling by IHC and Western blot analysis in these patient-derived mCRPC models (PDXs) and showed increases in phosphorylated-HER3, AR-V7 and phosphorylated-AKT in castrated CP50 adenocarcinoma model in keeping with previous reports *(Figure 2A and C)* (34). Conversely, we did not observe an increase in phosphorylated-HER3 or phosphorylated-AKT by Western blot analyses in CP142, the model with NE differentiation *(Figure 2B and D)* which has low HER3 protein expression.

10

RNAseq of these PDXs confirmed that HER2 and HER3 mRNA were highly expressed with lower EGFR, and minimal ERBB4 expression in both the intact and castrate states suggesting that HER2 may be the preferred HER3 dimerization partner. NRG1 and NRG2 mRNA was expressed at very low levels, both before and after castration *(Figure 2E-F)* although low levels of NRG1 protein were detected, *(Figure 2A-B and Supplementary Figure 3),* especially in castrated mice bearing CP142C suggesting possible upregulation of NRG1 expression after androgen deprivation in this model *(Figure 2C-D)*. Interestingly, these data also indicate post-transcriptional regulation of HER3 protein expression, with high HER3 mRNA but low HER3 protein in the model CP142. Overall, these data suggest that ligand independent, and/or ligand-dependent, HER3 heterodimerization and signaling may play an important biological role in castration resistance.

NRG1 expression in inflammatory cells, in prostate cancer biopsies

Ligand-induced activation of HER3 by neuregulins plays a key role in driving proliferation in HER3 positive tumors and has been recently suggested to play a role in PC biology in a subpopulation of PC (35). To gain further insights into the potential clinical significance of this axis in PC we studied the immunohistochemical expression of the predominant neuregulin, NRG1, utilizing a validated assay (*Supplementary Figure 3*) in a cohort of PC biopsies (n=46) and found that both CSPC and CRPC tumors had low NRG1 cytoplasmic staining by immunohistochemistry *(Supplementary Figure 4B, left panel, and Figure 3A),* similar to what was seen in our PDXs, with no discernible nuclear or membranous accentuation and little RNA*ish* positive staining (*Supplementary Figures 4A-B)*. Interestingly, there were no detectable differences between tumor cell NRG1 protein expression in CSPC and CRPC. NRG1 staining in the peritumoral stroma, however, showed greater variability based on cell type and intensity of expression. We, however, surprisingly observed NRG1 positivity in peritumoral inflammatory cells including neutrophils as well as intratumor myeloid cells with interestingly NRG1 protein levels in inflammatory cells being significantly higher in CRPC samples than those present in CSPC suggesting that castration induces NRG1 expressing myelomonocytic cell recruitment *(Figure 3A-B)*. NRG1 expression was detectable in stromal fibroblasts as previously described (36), albeit at much lower intensity and sparser density in the peritumoral stroma compared with inflammatory cells. NRG1 staining intensity in cells in the tumor stroma was usually stronger than seen in PC *(Supplementary Figures 4B, left panel)*. Further evaluation using multicolor immunofluorescence (IF) confirmed the high expression of NRG1 in CD11b positive myelomonocytic inflammatory cells as well as CD68 expressing cells *(Figure 3A).* Consistent with paracrine secretion of NRG1 by this inflammatory component, we performed Western blot analyses of NRG1 utilizing mononuclear cells from apheresis products from CRPC patients (n=9) and confirmed NRG1 expression in circulating mononuclear cells *(Supplementary Figure 4C)*.

11

We next analyzed single-cell RNAseq profiles from an independent cohort of 13 prostate tumor samples, recently published and publicly available (19), and confirmed that the highest levels of NRG1 mRNA were present in CD11b and CD68 positive clusters, with high expression also detected in a TP63 cell cluster, in keeping with basal-like tumor cell expression of NRG1 *(Figure 3C-F and Supplementary Figure 4E)*. Overall, these data surprisingly indicate that NRG1 expression in lethal PC is primarily generated by myelomonocytic inflammatory cells.

NRG1 and myelomonocytic cells in a transgenic PC model

To unravel the role of immune cell infiltrates in paracrine NRG1 secretion, we next investigated single cell RNAseq data generated from prostatic tumors resected from *Pten$^{-/-}$* transgenic mice, disaggregated into single cell suspensions and then FACS sorted using established lineage markers. These data confirmed that myelomonocytic cells including FACS sorted cell subtypes of monocytic-MDSCs (M-MDSCs) and macrophages expressed the highest levels of *NRG1* mRNA in transgenic models while peripheral mononuclear cell MDSCs (PMN-MDSCs) and stromal cells expressed lower but detectable levels of *NRG1 (Figure 3F)*. These data also supported NRG1 as the predominant expressed cytokine over NRG2. We consistently confirmed that NRG1 RNA and protein were primarily expressed by murine BM-derived precursors including M-MDSCs, PMN-MDSCs and macrophages by Western blot and RNAseq analyses *(Figure 3G and Supplementary Figure 4D)*. To study whether NRG1 secretion by myelomonocytic cells fuels PC growth, mouse PC organoids (*Pten$^{-/-}$Trp53$^{-/-}$*) were exposed to conditioned media from their sorted, cultured, MDSCs and macrophages (28,29). These conditioned media significantly increased the proliferation of murine PC organoids, with this being reversed by a neutralizing anti-NRG1 antibody, suggesting that PC growth is at least in part mediated by paracrine NRG1 secretion generated by these myelomonocytic cells *(Figure 3H-I and Supplementary Table 3)*. Overall, these data provided further evidence that myelomonocytic inflammatory cells generate paracrine NRG1 that activates HER3 heterodimerization and signaling in prostate cancer.

HER3 activation promotes growth in patient-derived organoid models of prostate cancer

We next studied whether NRG1-mediated HER3 activation impacts the growth of human mCRPC PDX-O models *in vitro (Figure 4A)*. We demonstrated that the addition of recombinant NRG1 (rNRG1) to these organoid cultures substantially increased cell growth in the HER3 positive model CP50, where a 2-fold increase in cell proliferation was observed, with the formation of larger and morphologically distinctive organoids comprising bigger cellular areas *(Supplementary Figure 5A)*

12

(37). This effect was not observed in the HER3 low model CP142 PDX-Os. NRG1-mediated HER3 activation was demonstrated by pHER3 expression in CP50 PDX-O model by WB *(Figure 4A, right)* and with increasing concentrations of NRG1 *in vitro* that being reversed with anti-HER3 antibody (U3-1287-Patritumab) *(Supplementary Figure 5B).* Overall, these data suggested that NRG1 activation of HER3 may increase prostate cancer growth in a ligand-dependent manner.

Targeting HER3 in vitro and in vivo in patient-derived models and cell lines

Targeting ERBB signaling in clinical trials has to date failed to impart patient benefit, perhaps due to feedback loops, continued AR signaling, or insufficient blockade of the entire ERBB axis (9,10). To circumvent these challenges, we elected to study the antitumor activity of not only the anti-HER3 antibody patritumab but also of the anti-HER3 antibody-drug conjugate (ADC) U3-1402 (Daiichi Sankyo), in our PC cell lines and PDX-O models *in vitro*. This ADC (U3-1402) is in early clinical trials (NCT02204345, NCT02980341) (11) and comprises of an anti-HER3 antibody joined, via a peptide-based linker, to a topoisomerase-1-inhibitor payload (DXd) which will generate double strand DNA breaks that can result in tumor kill (38). The antitumor activity of U3-1402 was compared to that of the parental anti-HER3 antibody (patritumab) and a control, non-targeted, IgG-ADC (MAAA-9289) conjugated to payload Dxd. Single agent HER3 targeting by patritumab alone had antitumor activity *in vitro* in the HER3 high expressing CP50 patient-derived model *(Figures 4B)*, but little antitumor activity against the HER3 positive prostate cancer cells lines LnCaP, LnCaP95 and 22RV1 (*Supplementary Figure 5C-D*), perhaps indicating that the development of HER3 targeting agent requires rational combination studies targeting all active ERBB receptors as well as the androgen receptor. Patritumab also had little antitumor activity against the HER3 low CP142 model *in vitro* *(Figures 4B)*. Conversely, the anti-HER3 immunoconjugate U3-1402 had antitumor activity in the *in vitro* model CP50 *(Figures 4B)* and the HER3-positive prostate cancer cell lines (LNCap, LNCap95 and 22Rv1) *(Supplementary Figure 5D)*. Interestingly, both the anti-HER3 antibody (patritumab) (39) and the anti-HER3 ADC (U3-1402) had *in vitro* antitumor activity against the HER3 high PDX-O CP50, suggesting signaling inhibition in this model impacts tumor growth *(Figure 4B, left panel)*. Of note, some off target antitumor activity was observed with the IgG-ADC control *in vitro* in the CP142-PDX-O model and LNCap95 cell line tested suggesting payload drug sensitivity for these tumor cells at higher doses *(Figure 4B and Supplementary Figure 5D)*. The HER3-dependent response of U3-1402 was supported by the limited antitumor activity of the ADC observed in the HER3-low model CP142 *in vitro* (40) *(Figure 4B, right panel)*.

We finally evaluated the *in vivo* antitumor activity of U3-1402 and patritumab in the HER3-positive and ATM deficient mCRPC PDX model CP50, which originated from a patient who had progressed

13

through all standard of care therapies including docetaxel, cabazitaxel, abiraterone and enzalutamide (16). U3-1402 demonstrated potent and sustained antitumor activity when utilizing a weekly dosing regimen at 10mg/kg for a total of five doses *(Figure 4C, left panel)*. U3-1402 was effective without inducing any body weight loss or apparent toxicity in these mice. Additionally, no tumor regrowth was observed up to 60-days following the end of dosing. Patritumab demonstrated little antitumor activity in this model suggesting that blocking HER3 alone may not have antitumor activity *in vivo* while the cytotoxin (Dxd) linked to a non-specific antibody (MAAA-9829) also displayed minimal antitumor activity indicating HER3-dependent targeting. We also studied the low HER3 expressing *in vivo* model CP142-PDX treated with the same dose (10mg/Kg) of U3-1402 weekly for a total of three doses and observed that U3-1402 and patritumab had minimal antitumor activity in this model *(Figure 4C, right panel)* highlighting the relevance of high HER3 expression as a functional therapeutic target of U3-1402.

DISCUSSION

There remains an urgent need to develop new therapeutic strategies to improve outcome from advanced PC (41). Twenty years ago, studies implicated HER2 signaling as a mechanism for endocrine treatment resistance in models of PC (6). This led to the conduct of multiple clinical trials for men suffering from mCRPC using ERBB targeting drugs including pertuzumab and afatinib but these demonstrated little antitumor activity as single agents (7,8). While these trials predated the identification of continued AR signaling as a cause of castration resistance, and clinical studies with abiraterone and enzalutamide (42), they discredited targeting ERBB signaling as a therapeutic strategy for mCRPC. More recent studies have implicated the NRG1/HER3 axis as playing a role in PC biology, suggesting that neuregulin is fibroblast generated (34). We now provide strong evidence to further validate HER3 as a therapeutic target for the treatment of advanced prostate cancer, demonstrating that: 1) its overexpression associates with poorer time to castration resistance and worse overall survival and higher Ki67; 2) confirming that androgen deprivation can increase HER3 phosphorylation in patient-derived xenograft models *in vivo*; 3) the HER3 ligand NRG1 is primarily paracrine and mostly expressed by inflammatory myelomonocytic cells, increasing patient-derived model growth in HER3-expressing tumors; 4) that while *in vitro* targeting of HER3 signaling has antitumor activity, *in vivo* targeting of HER3 signaling has minimal impact on tumor growth possibly due to the release of other paracrine factors such as IL-23 by myelomonocytic cells (23); 5) but that an anti-HER3 immunoconjugate with a topoisomerase-1 inhibitor payload has impressive and durable antitumor activity against prostate cancer models expressing high (but not low) levels of HER3 with little antitumor activity from a non-specific antibody immunoconjugate with the same payload.

14

HER3 is largely considered a kinase-dead receptor due to alterations of conserved residues in the catalytic domain (43), though evidence exists for HER3 auto-phosphorylation indicating that this receptor may preserve some weak kinase activity (44). HER3 largely signals through heterodimerization with other ERBB receptors, although heterodimerization with non-canonical receptors has been suggested (33,45). Interestingly, we demonstrate an increase in HER2 expression at castration resistance and also demonstrate that in patient biopsies and transgenic mouse models of prostate cancer that NRG1 is largely generated by myelomonocytic inflammatory cells which increase with castration resistance; these have been previously demonstrated to be chemoattracted down a chemokine gradient into prostate cancer stroma after androgen deprivation and to fuel PC cell proliferation and tumor growth by secreting paracrine factors including IL-23 which we have shown to upregulate AR signaling (28,29) Unlike IL-23, NRG1-activated HER3 activates AKT signaling by preferentially heterodimerizing with HER2 through HER3 phosphorylation (32,46). Overall, this suggests that chemoattracted myelomonocytic cells can release paracrine factors that activate both AR and AKT signaling.

We also demonstrate in the studies herein that in mCRPC while both HER2 and HER3 mRNAs are highly co-overexpressed, HER2 protein is expressed at much lower levels although it increases at castration resistance. We also demonstrate HER3 signaling activation in our PDX models *in vivo* upon castration. We have, however, been unable to disprove ligand independent HER3 activation, but have demonstrated little evidence for autocrine tumor cell generation of the high affinity HER3 neuregulin ligands NRG1 and NRG2 by immunohistochemistry and RNA*ish* in adenocarcinoma although our studies suggest that neuroendocrine PC cells may express NRG1. Furthermore, we could not identify any cases of NRG1 fusions/translocations in available mCRPC genomic data as has been suggested for other cancers and at least one case of prostate cancer (47).

We do, however, show that in patient-derived mCRPC models HER3 paracrine activation by NRG1, increases tumor growth (36). Overall, these results have led to our routine use of rNRG1 in mCRPC organoid cultures to enable their longer-duration culture which had been a major challenge (48). Our data indicate paracrine NRG1 in lethal prostate cancer is primarily generated by inflammatory cells, although some fibroblast NRG1 expression was also detected. NRG1 staining in the peritumoral stroma was observed in lymphocytes, histiocytes and mature neutrophils. This was supported by studies of BM precursors from PC transgenic models (49).

Since HER3 activation activates PI3K/AKT activation and other signaling pathways, inhibition of myelomonocytic cell generated NRG1-induced HER3 activity is worth pursuing in clinical studies. However, it is likely that blockade of not only ERBB signaling but also of other paracrine factors released by myelomonocytic cells including IL-23, which fuels androgen receptor and androgen receptor splice variant signaling through RORγ, will be required to generate tumor cell kill. Thus, we

evaluated the antitumor activity of not only the anti-HER3 antibody patritumab but also of U3-1402, an anti-HER3 antibody-drug-conjugate (ADC) linked to a topoisomerase-1 inhibitor exatecan derivative (Dxd); this significantly inhibited tumor growth in multiple HER3-expressing model with little antitumor activity in a HER3 low model. We acknowledge that further studies of drug combinations incorporating HER3/ERBB inhibitor combinations are warranted, such as the co-targeting of IL-23/IL-23R/RORγ and HER3 signaling with the absence of these data being a limitation of our studies.

In conclusion, the data herein indicate that HER3 has clinical relevance in lethal PC where it is commonly expressed, being most likely activated in mCRPC by NRG1 secreted from myelomonocytic cells. We also present data indicating that HER3 merits targeting by anti-HER3 immunoconjugate therapy in clinical trials for men suffering from high HER3 expressing lethal PC and envision that these can add PC to the list of common tumors that can be treated by ERBB targeting strategies.

ACKNOWLEDMENTS

REFERENCES

1. Sartor O, de Bono JS. Metastatic Prostate Cancer. N Engl J Med **2018**;378:1653-4

2. Armenia J, Wankowicz SAM, Liu D, Gao J, Kundra R, Reznik E*, et al.* The long tail of oncogenic drivers in prostate cancer. Nat Genet **2018**;50:645-51

3. Robinson D, Van Allen EM, Wu YM, Schultz N, Lonigro RJ, Mosquera JM*, et al.* Integrative Clinical Genomics of Advanced Prostate Cancer. Cell **2015**;162:454

4. Sharp A, Coleman I, Yuan W, Sprenger C, Dolling D, Rodrigues DN*, et al.* Androgen receptor splice variant-7 expression emerges with castration resistance in prostate cancer. J Clin Invest **2019**;129:192-208

5. Einstein DJ, Arai S, Balk SP. Targeting the androgen receptor and overcoming resistance in prostate cancer. Current opinion in oncology **2019**;31:175-82

6. Craft N, Shostak Y, Carey M, Sawyers CL. A mechanism for hormone-independent prostate cancer through modulation of androgen receptor signaling by the HER-2/neu tyrosine kinase. Nature medicine **1999**;5:280-5

7. Molife LR, Omlin A, Jones RJ, Karavasilis V, Bloomfield D, Lumsden G*, et al.* Randomized Phase II trial of nintedanib, afatinib and sequential combination in castration-resistant prostate cancer. Future oncology (London, England) **2014**;10:219-31

8. de Bono JS, Bellmunt J, Attard G, Droz JP, Miller K, Flechon A*, et al.* Open-label phase II study evaluating the efficacy and safety of two doses of pertuzumab in castrate chemotherapy-naive patients with hormone-refractory prostate cancer. Journal of clinical oncology : official journal of the American Society of Clinical Oncology **2007**;25:257-62

9. Slamon D, Clark G, Wong S, Levin W, Ullrich A, McGuire W. Human breast cancer: correlation of relapse and survival with amplification of the HER-2/neu oncogene. Science **1987**;235:177-82

10. Koumakpayi IH, Diallo J-S, Le Page C, Lessard L, Gleave M, Bégin LR*, et al.* Expression and Nuclear Localization of ErbB3 in Prostate Cancer. Clinical Cancer Research **2006**;12:2730

11. Masuda N, Yonemori K, Takahashi S, Kogawa T, Nakayama T, Iwase H*, et al.* Abstract PD1-03: Single agent activity of U3-1402, a HER3-targeting antibody-drug conjugate, in HER3-overexpressing metastatic breast cancer: Updated results of a phase 1/2 trial. Cancer Research **2019**;79:PD1-03-PD1-

12. Poovassery JS, Kang JC, Kim D, Ober RJ, Ward ES. Antibody targeting of HER2/HER3 signaling overcomes heregulin-induced resistance to PI3K inhibition in prostate cancer. Int J Cancer **2015**;137:267-77

13. Tamura K, Tsurutani J, Takahashi S, Iwata H, Krop IE, Redfern C*, et al.* Trastuzumab deruxtecan (DS-8201a) in patients with advanced HER2-positive breast cancer previously treated with trastuzumab emtansine: a dose-expansion, phase 1 study. Lancet Oncol **2019**

14. Mateo J, Carreira S, Sandhu S, Miranda S, Mossop H, Perez-Lopez R*, et al.* DNA-Repair Defects and Olaparib in Metastatic Prostate Cancer. N Engl J Med **2015**;373:1697-708

15. Welti J, Sharp A, Brooks N, Yuan W, McNair C, Chand SN*, et al.* Targeting p300/CBP axis in lethal prostate cancer. Cancer Discov **2021**

16. Welti J, Sharp A, Yuan W, Dolling D, Nava Rodrigues D, Figueiredo I*, et al.* Targeting Bromodomain and Extra-Terminal (BET) Family Proteins in Castration-Resistant Prostate Cancer (CRPC). Clin Cancer Res **2018**;24:3149-62

17. Workman P, Aboagye EO, Balkwill F, Balmain A, Bruder G, Chaplin DJ*, et al.* Guidelines for the welfare and use of animals in cancer research. British Journal Of Cancer **2010**;102:1555

18. Drost J, Karthaus WR, Gao D, Driehuis E, Sawyers CL, Chen Y*, et al.* Organoid culture systems for prostate epithelial and cancer tissue. Nat Protoc **2016**;11:347-58

19. Chen S, Zhu G, Yang Y, Wang F, Xiao YT, Zhang N*, et al.* Single-cell analysis reveals transcriptomic remodellings in distinct cell types that contribute to human prostate cancer progression. Nat Cell Biol **2021**;23:87-98

20. Wolf FA, Angerer P, Theis FJ. SCANPY: large-scale single-cell gene expression data analysis. Genome Biol **2018**;19:15

21.   Polanski K, Young MD, Miao Z, Meyer KB, Teichmann SA, Park JE. BBKNN: fast batch alignment of single cell transcriptomes. Bioinformatics **2020**;36:964-5

22.   Traag VA, Waltman L, van Eck NJ. From Louvain to Leiden: guaranteeing well-connected communities. Sci Rep **2019**;9:5233

23.   Aran D, Looney AP, Liu L, Wu E, Fong V, Hsu A*, et al.* Reference-based analysis of lung single-cell sequencing reveals a transitional profibrotic macrophage. Nat Immunol **2019**;20:163-72

24.   Martens JH, Stunnenberg HG. BLUEPRINT: mapping human blood cell epigenomes. Haematologica **2013**;98:1487-9

25.   de Souza N. The ENCODE project. Nat Methods **2012**;9:1046

26.   McInnes L, Healy J, Melville J. Umap: Uniform manifold approximation and projection for dimension reduction. arXiv preprint arXiv:180203426 **2018**

27.   Becht E, McInnes L, Healy J, Dutertre CA, Kwok IWH, Ng LG*, et al.* Dimensionality reduction for visualizing single-cell data using UMAP. Nat Biotechnol **2018**

28.   Di Mitri D, Mirenda M, Vasilevska J, Calcinotto A, Delaleu N, Revandkar A*, et al.* Re-education of Tumor-Associated Macrophages by CXCR2 Blockade Drives Senescence and Tumor Inhibition in Advanced Prostate Cancer. Cell Rep **2019**;28:2156-68 e5

29.   Calcinotto A, Spataro C, Zagato E, Di Mitri D, Gil V, Crespo M*, et al.* IL-23 secreted by myeloid cells drives castration-resistant prostate cancer. Nature **2018**;559:363-9

30.   Trapnell C, Roberts A, Goff L, Pertea G, Kim D, Kelley DR*, et al.* Differential gene and transcript expression analysis of RNA-seq experiments with TopHat and Cufflinks. Nature protocols **2012**;7:562-78

31.   Chen L, Siddiqui S, Bose S, Mooso B, Asuncion A, Bedolla RG*, et al.* Nrdp1-mediated regulation of ErbB3 expression by the androgen receptor in androgen-dependent but not castrate-resistant prostate cancer cells. Cancer Res **2010**;70:5994-6003

32.   Junttila TT, Akita RW, Parsons K, Fields C, Lewis Phillips GD, Friedman LS*, et al.* Ligand-independent HER2/HER3/PI3K complex is disrupted by trastuzumab and is effectively inhibited by the PI3K inhibitor GDC-0941. Cancer Cell **2009**;15:429-40

33.   Yarden Y, Sliwkowski MX. Untangling the ErbB signalling network. Nat Rev Mol Cell Biol **2001**;2:127-37

34.   Carver Brett S, Chapinski C, Wongvipat J, Hieronymus H, Chen Y, Chandarlapaty S*, et al.* Reciprocal Feedback Regulation of PI3K and Androgen Receptor Signaling in PTEN-Deficient Prostate Cancer. Cancer Cell **2011**;19:575-86

35.   Mota JM, Collier KA, Barros Costa RL, Taxter T, Kalyan A, Leite CA*, et al.* A comprehensive review of heregulins, HER3, and HER4 as potential therapeutic targets in cancer. Oncotarget **2017**;8:89284-306

36.   Zhang Z, Karthaus WR, Lee YS, Gao VR, Wu C, Russo JW*, et al.* Tumor Microenvironment-Derived NRG1 Promotes Antiandrogen Resistance in Prostate Cancer. Cancer Cell **2020**;38:279-96 e9

37.   Ku SY, Rosario S, Wang Y, Mu P, Seshadri M, Goodrich ZW*, et al.* Rb1 and Trp53 cooperate to suppress prostate cancer lineage plasticity, metastasis, and antiandrogen resistance. Science **2017**;355:78-83

38.   Yonesaka K, Takegawa N, Watanabe S, Haratani K, Kawakami H, Sakai K*, et al.* An HER3-targeting antibody-drug conjugate incorporating a DNA topoisomerase I inhibitor U3-1402 conquers EGFR tyrosine kinase inhibitor-resistant NSCLC. Oncogene **2019**;38:1398-409

39.   Shimizu T, Yonesaka K, Hayashi H, Iwasa T, Haratani K, Yamada H*, et al.* Phase 1 study of new formulation of patritumab (U3-1287) Process 2, a fully human anti-HER3 monoclonal antibody in combination with erlotinib in Japanese patients with advanced non-small cell lung cancer. Cancer chemotherapy and pharmacology **2017**;79:489-95

40.   Hashimoto Y, Koyama K, Kamai Y, Hirotani K, Ogitani Y, Zembutsu A*, et al.* A Novel HER3-Targeting Antibody–Drug Conjugate, U3-1402, Exhibits Potent Therapeutic Efficacy through the Delivery of Cytotoxic Payload by Efficient Internalization. Clinical Cancer Research **2019**;25:7151

18

41.   Yap TA, Smith AD, Ferraldeschi R, Al-Lazikani B, Workman P, de Bono JS. Drug discovery in advanced prostate cancer: translating biology into therapy. Nature reviews Drug discovery **2016**;15:699-718

42.   de Bono JS, Logothetis CJ, Molina A, Fizazi K, North S, Chu L*, et al.* Abiraterone and Increased Survival in Metastatic Prostate Cancer. New England Journal of Medicine **2011**;364:1995-2005

43.   Xie T, Lim SM, Westover KD, Dodge ME, Ercan D, Ficarro SB*, et al.* Pharmacological targeting of the pseudokinase Her3. Nat Chem Biol **2014**;10:1006-12

44.   Shi F, Telesco SE, Liu Y, Radhakrishnan R, Lemmon MA. ErbB3/HER3 intracellular domain is competent to bind ATP and catalyze autophosphorylation. Proceedings of the National Academy of Sciences **2010**;107:7692

45.   Li C, Wang S, Xing Z, Lin A, Liang K, Song J*, et al.* A ROR1-HER3-lncRNA signalling axis modulates the Hippo-YAP pathway to regulate bone metastasis. Nat Cell Biol **2017**;19:106-19

46.   Hsieh AC, Moasser MM. Targeting HER proteins in cancer therapy and the role of the non-target HER3. Br J Cancer **2007**;97:453-7

47.   Ptakova N, Martinek P, Holubec L, Janovsky V, Vancurova J, Grossmann P*, et al.* Identification of tumors with NRG1 rearrangement, including a novel putative pathogenic UNC5D-NRG1 gene fusion in prostate cancer by data-drilling a de-identified tumor database. Genes Chromosomes Cancer **2021**

48.   Puca L, Bareja R, Prandi D, Shaw R, Benelli M, Karthaus WR*, et al.* Patient derived organoids to model rare prostate cancer phenotypes. Nature Communications **2018**;9:2404

49.   Revandkar A, Perciato ML, Toso A, Alajati A, Chen J, Gerber H*, et al.* Inhibition of Notch pathway arrests PTEN-deficient advanced prostate cancer by triggering p27-driven cellular senescence. Nat Commun **2016**;7:13719

19

FIGURE LEGENDS

Figure 1: HER3 expression in lethal prostate cancer has clinical relevance.
(A-B) Transcriptome analyses of RNAseq data from 159 mCRPC biopsies (PCF/SU2C International Prostate Cancer Dream Team) for ERBB family member expression (Fragments Per Kilobase of transcript per Million (FPKM)) **(A)** and comparison of ERBB3/HER3 (X-axis) and ERBB2/HER2 (y-axis) mRNA expression in same patient samples showing a statistically significant positive correlation (Spearman r=0.4370928) **(B)**. **(C)** Representative IHC images of HER2 (left panel) and HER3 (right panel) protein detection in same-patient CSPC and CRPC biopsies (scale bar 100μm) with membranous OD shown for each in top right corners. **(D)** Kaplan-Meier curves for time to CRPC from diagnosis of prostate cancer for membranous HER2 expression by median OD (155.5) (left) and membranous HER3 expression by median OD (2958.0) (right). HER3 but not HER2 protein expression by IHC associates with time to CRPC. Hazard ratio (HR) with 95% confidence intervals and p-values for univariate cox survival model are shown. **(E)** Kaplan-Meier curves for overall survival (OS), from diagnosis of prostate cancer for membranous HER2 expression by median OD (155.5) (left) and membranous HER3 expression by median OD (2958.0) (right). HER3 but not HER2 protein expression by IHC associates with OS. Hazard ratio (HR) with 95% confidence intervals and p-values for univariate cox survival model are shown.

Figure 2: Upregulation of HER3 expression in CRPC models.
(A-B) AR, ARv7, EGFR, HER2, HER3 and NRG1 protein expression by IHC on PDX tumor samples developed in intact and castrated mice for CP50 **(A)**, CP142 **(B)** (scale bar 50μm). **(C-D)** Western blot showing AR, ARv7, NRG1 and ERBB receptors expression and phospho-AKT pathway activation, in same models as A to B. Proteins below detection level represented as n.d. **(E-F)** Transcriptome analyses of RNAseq data on intact (n= 3, left) and castrate (n= 3, right) PDX tumor samples, for ERBB family member and NRG1 and NRG2 ligands expression (FPKM), divided into very high (upper 25% expressed genes), medium high (50%-75% expressed genes), medium low (25%-50% expressed genes) and very low (lower 25% expressed genes), in same models as A and B.

Figure 3: NRG-activated HER3 signaling in lethal PC. (A) Representative micrographs of PC patient samples, showing NRG1 protein expression, by IHC and IF, in CD11b (green) and CD68 (yellow) positive inflammatory cells. Scale bar 50μm. **(B)** NRG1 protein expression,

20

by IHC, in prostatic adenocarcinoma samples, CSPC (left, n=24) and CRPC (right, n=34), showing significantly higher expression in inflammatory cells (red) compared to tumor (grey) (Mann-Whitney test, p values: *p≤0.05, **p≤0.01, ***p≤0.001 and ****p≤0.0001, median H-score and interquartile range shown) and showing significantly higher expression in inflammatory cells present in CRPC, compared to inflammatory cells present in CSPC, no significant differences observed between CSPC and CRPC tumor cells (Mann-Whitney test, p values: *p≤0.05, **p≤0.01, ***p≤0.001 and ****p≤0.0001). **(C)** UMAP projection of 30,329 single-cell gene expression profiles from twelve primary and one lymph node metastasis tissue samples (n=13) of 12 PC patients color-coded per sample. **(D)** Leiden algorithm identifies 8 clusters. Clusters are color-coded by SingleR-inferred cell subtype. **(E)** Violin plots depicting NRG1 expression levels per assigned cell subtype. **(F)** Violin plot representing frequency of immune, epithelial and stroma cells expressing NRG1 and NRG2 subtypes from FACS-sorted from murine prostate tumors Pten$^{-/-}$ followed by single cell transcriptome analysis (n=2). **(G)** RNAseq of FACS sorted murine BM-derived MDSCs, heatmap of log-CPM values for NRG1 genes in M-MDSCs, PMN-MDSCs and BM (n=3) (FDR adjusted, p<0.05). **(H)** Relative luminescence (RLU) as a measure for mouse prostate organoid proliferation within 5 days in conditional media generated from C57BL/6N mice BM-differentiated MDSCs and macrophages. Baseline organoid media as vehicle control with and without rNRG1. (Ordinary two-way ANOVA with Tukey's correction test, p values: *p≤0.05, **p≤0.01, ***p≤0.001 and ****p≤0.0001). **(I)** Experimental validation of functional NRG1 in conditional media from MDSCs and macrophages by antibody neutralization at 3µg (Heregulin 2573, Cell Signaling Technology). Luminescence readings at 5-days (Ordinary two-way ANOVA with Tukey's correction test, p values: *p≤0.05, **p≤0.01, ***p≤0.001 and ****p≤0.0001).

Figure 4: Anti-tumor activity of anti-HER3 antibody drug conjugate (ADC) U3-1402. (A) Organoid proliferation normalized to untreated vehicle in PDX-O models CP50 and CP142 (n=3) monitored for 7-days with and without additional rNRG1 (100ng/ml). ANOVA with Sidak's correction test was applied, p values: *p≤0.05, **p≤0.01, ***p≤0.001 and ****p≤0.0001 **(left)**, Immunoblots depicting phosphorylated-HER3 expression with additional rNRG1 in CP50 and CP142 PDX-O mCRPC models after 16h treatment with human rNRG1 (100ng/ml). GAPDH used as loading control **(right)**. **(B)** *In vitro* cell growth inhibitory activity of the anti-HER3 antibody-drug conjugate U3-1402 (red line) and the anti-HER3 antibody without payload U3-1287 (Patritumab; green line) in the PDX-O model CP50 (left) and CP142 (right), monitored for 7-days with endpoint assay

21

luminescence. All results are expressed as mean ± SEM (n=3). Statistical significance was analyzed using ANOVA with Dunnett's multiple comparisons correction test to analyze mean difference per concentration of U3-1402 and U3-1287 (Patritumab) vs IgG-ADC control (MAAA-9289, blue line), p values: *p≤0.05, **p≤0.01, ***p≤0.001 and ****p≤0.0001. **(C)** *In vivo* efficacy of the anti-HER3 antibody-drug conjugate U3-1402 (10mg/Kg, red line) in PDX models CP50 (left) and CP142 (right); the anti-HER3 antibody without payload U3-1287 (Patritumab; 10mg/Kg, green line) and IgG-ADC (MAAA-9289; 10mg/Kg, purple line) are also shown. CP50-PDX treated with U3-1402 was monitored for 5 weeks post-dosing (p values: *p≤0.05, **p≤0.01, ***p≤0.001 and ****p≤0.0001) and treatment was administered weekly for a total of five times (black arrows) while CP142-PDX received a total of three weekly doses. Vehicle, 10mM acetate buffer-5% sorbitol-pH 5.5 (blue line). All results were expressed as mean ± SEM (n=10) and statistical significance was analyzed using ANOVA with Dunnett multiple comparisons correction test to analyze mean difference of each treatment vs vehicle control 7-days post-treatment, corresponding to last tumor measurement.

Figure 1

A.

B.

p=8.4e−09

C.

D. Time to CRPC

E. Overall Survival
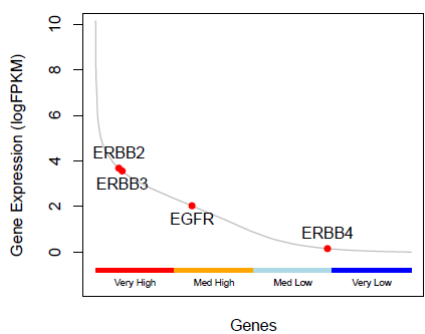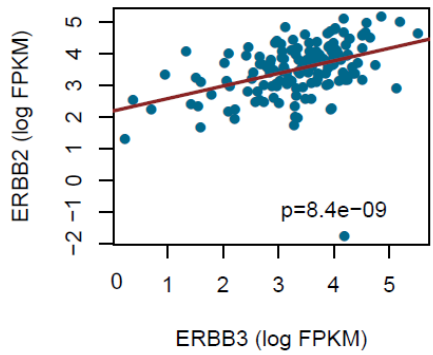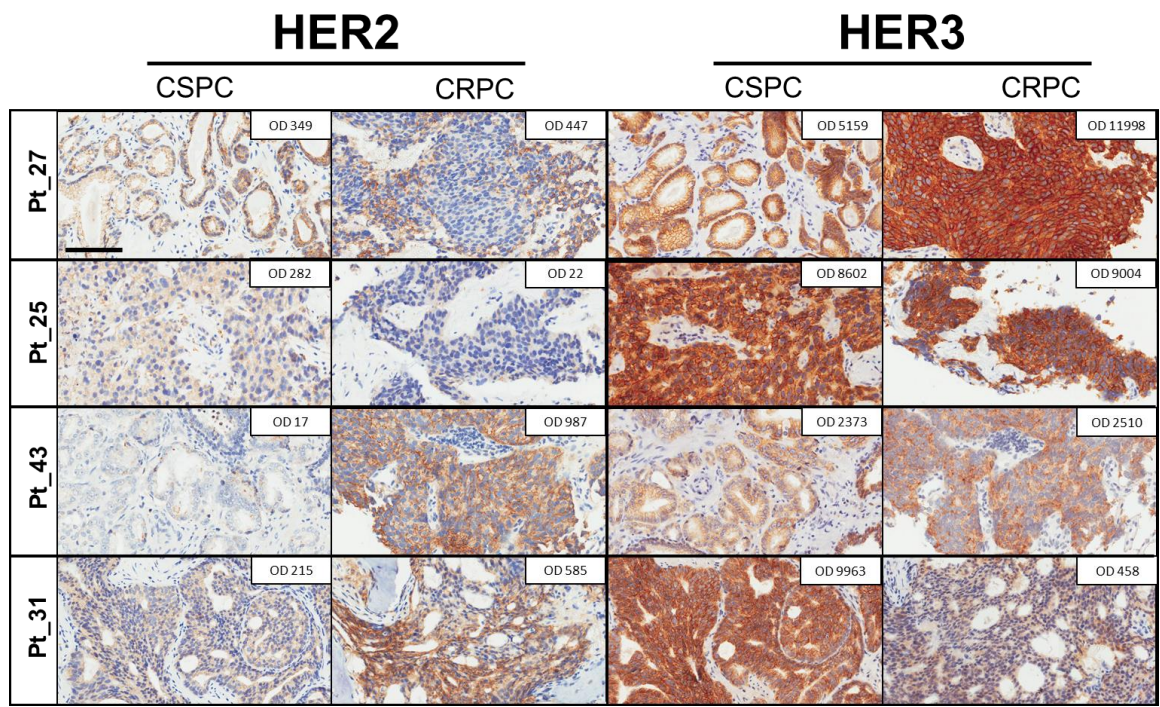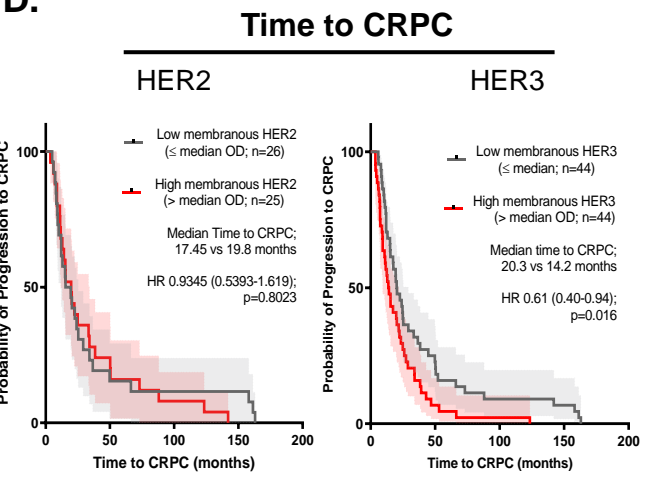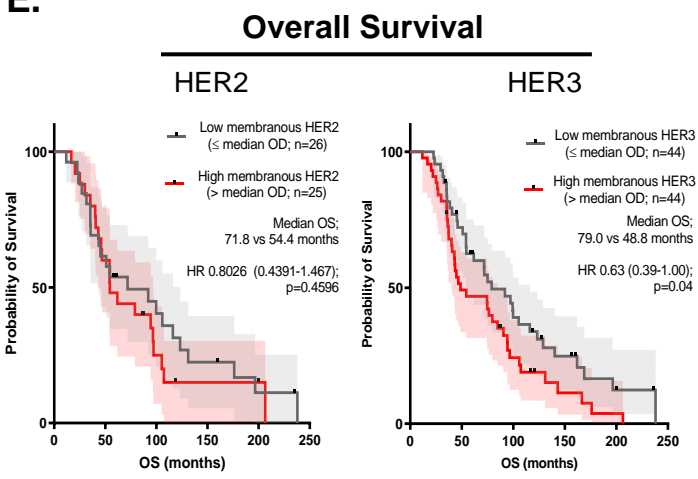
Figure 2

A.

B.

C.
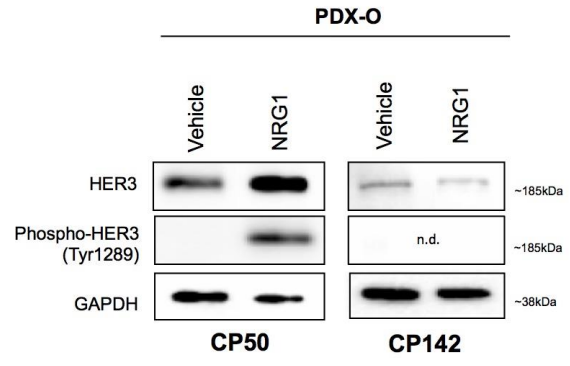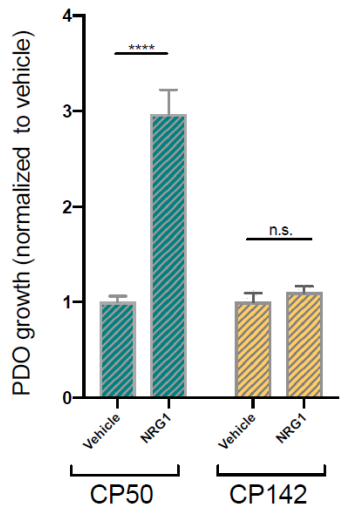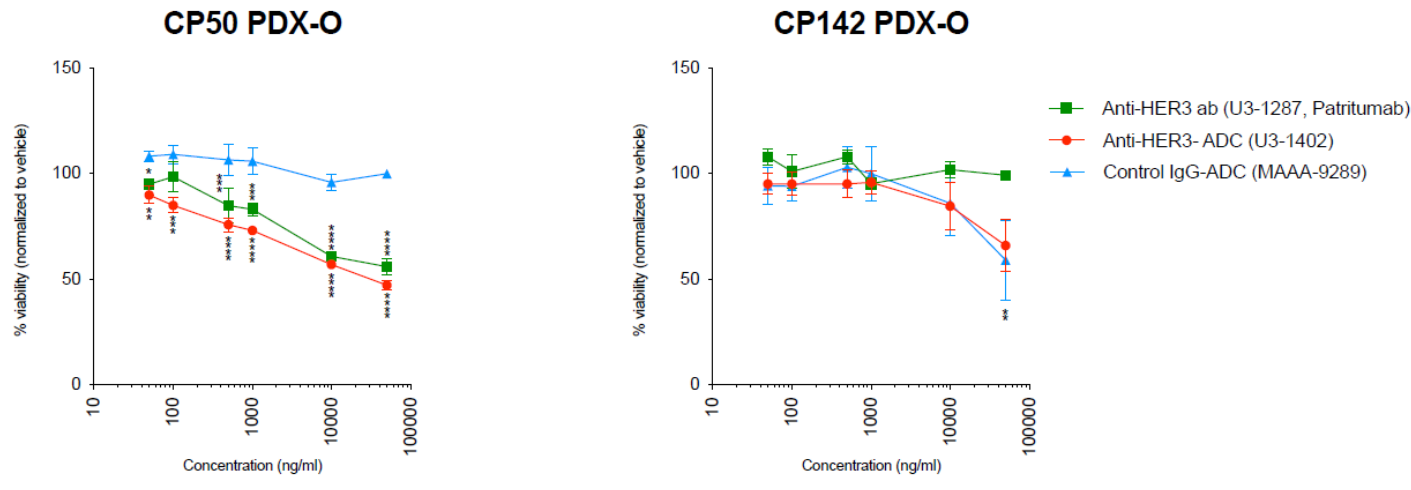

D.

E.

F.
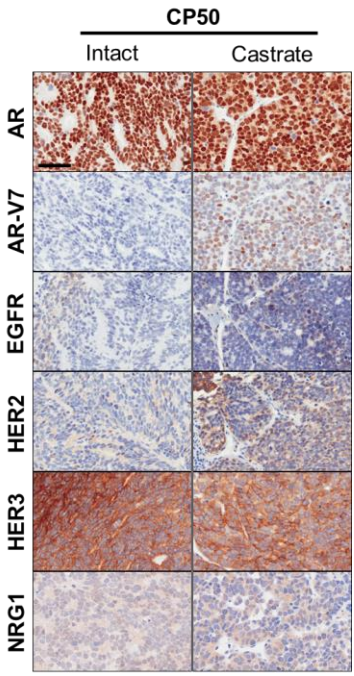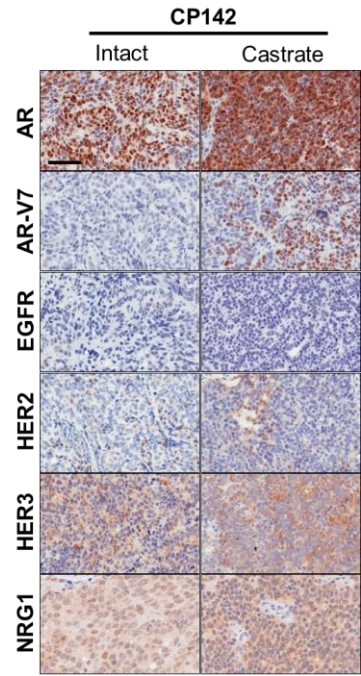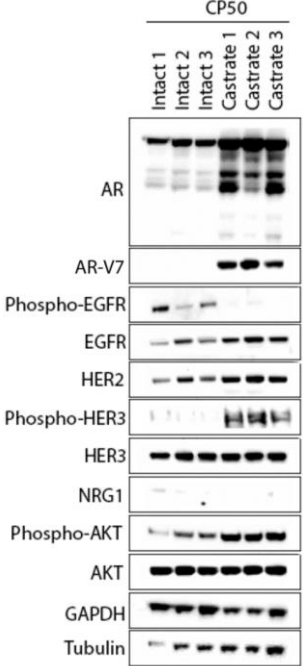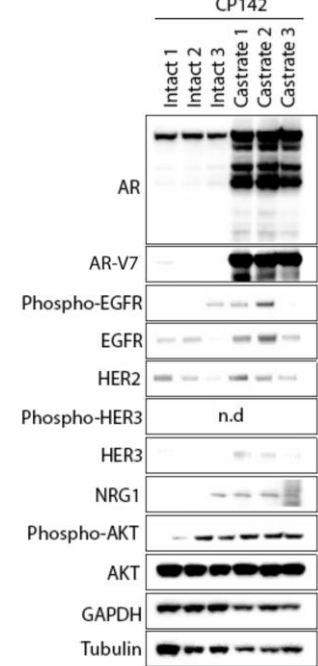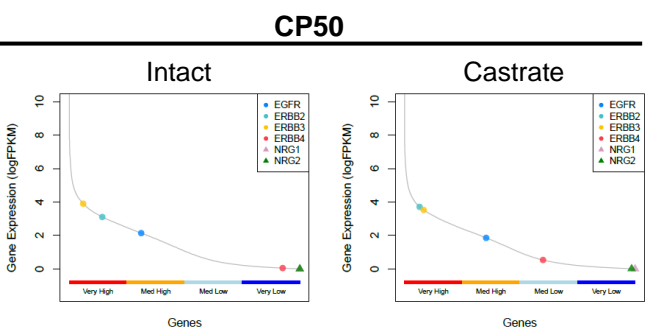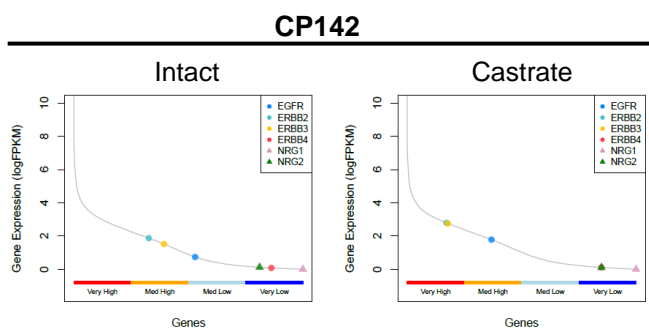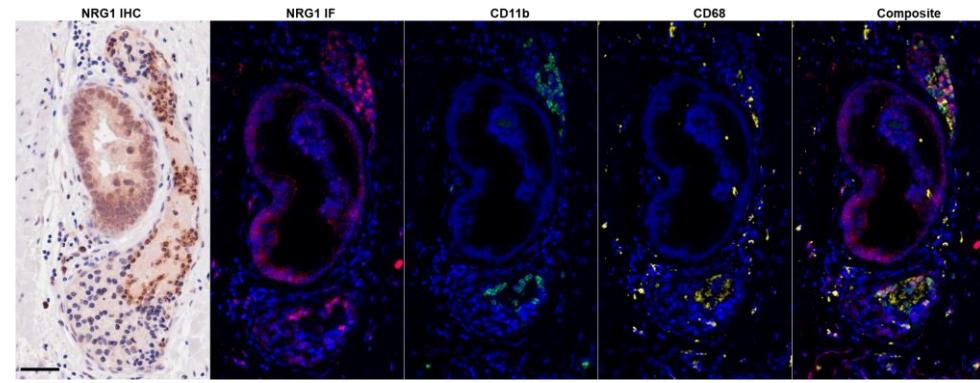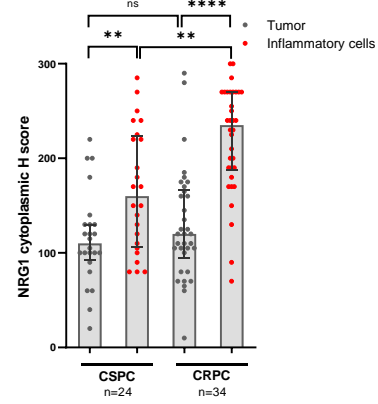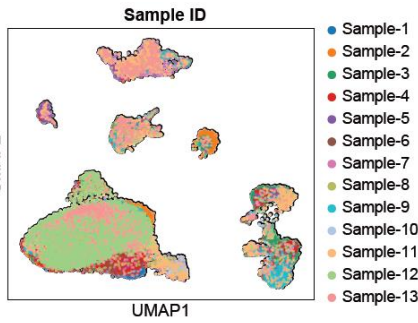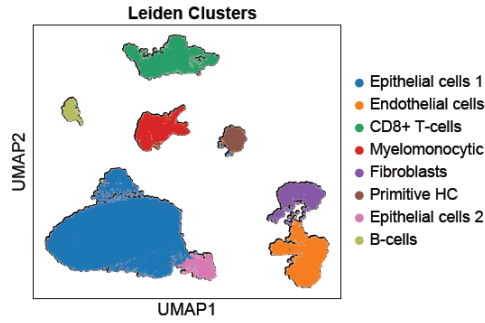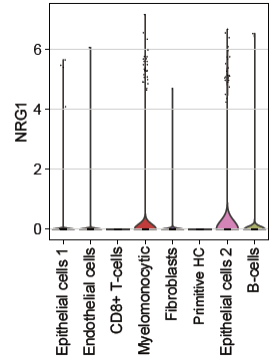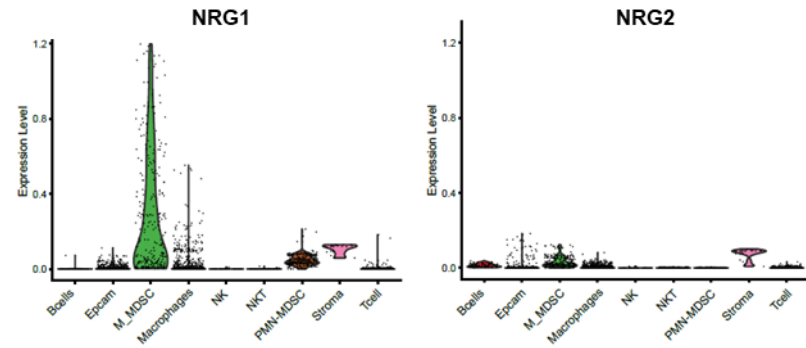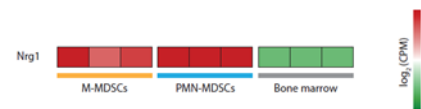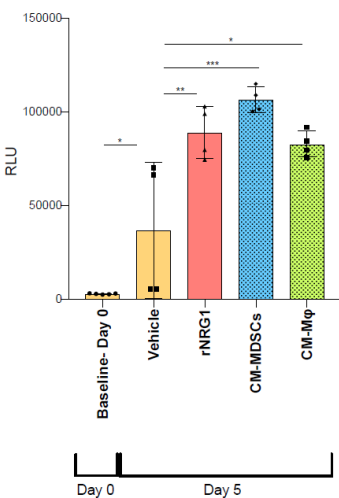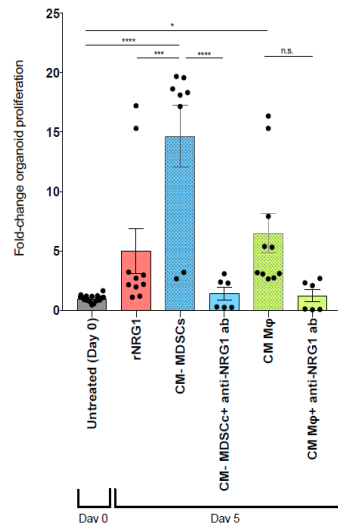
Figure 3

Figure 4

A.

B.
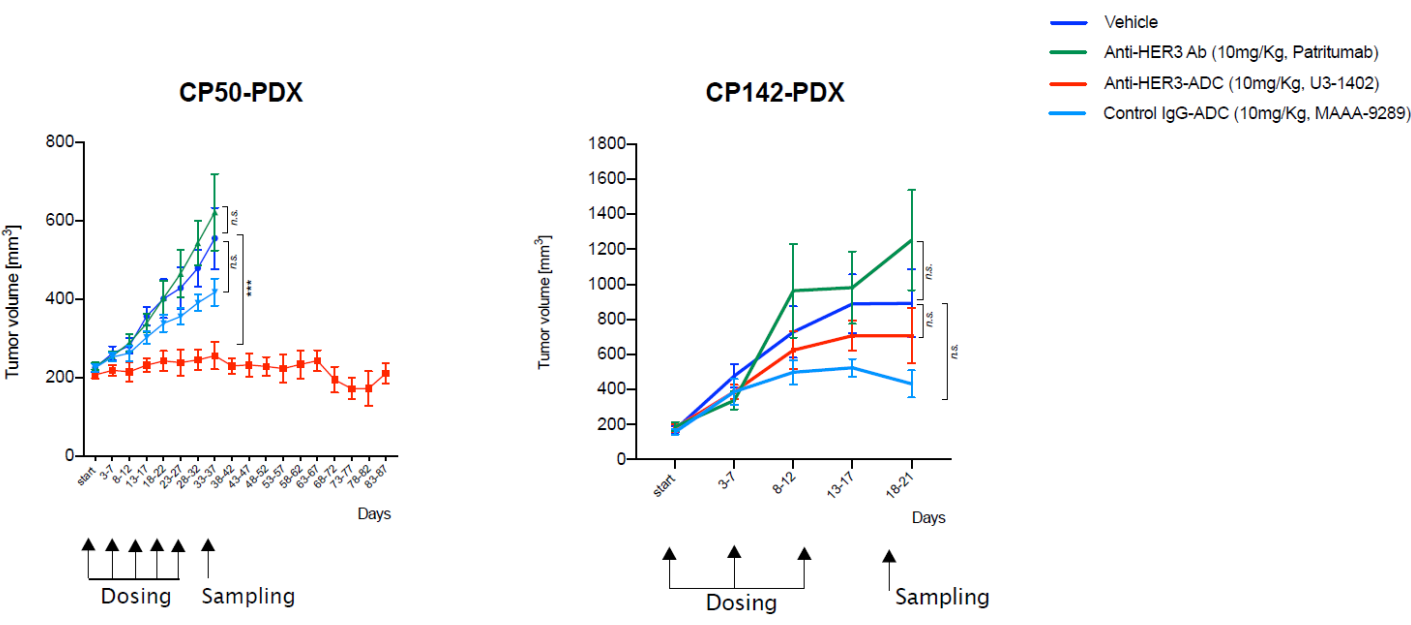

C.

Cancer Research

The Journal of Cancer Research (1916–1930) | The American Journal of Cancer (1931–1940)

AACR American Association for Cancer Research

HER3 is an Actionable Target in Advanced Prostate Cancer

Veronica Gil, Susana Miranda, Ruth Riisnaes, et al.

Updated version	Access the most recent version of this article at: doi:10.1158/0008-5472.CAN-21-3360
Supplementary Material	Access the most recent supplemental material at: http://cancerres.aacrjournals.org/content/suppl/2021/10/28/0008-5472.CAN-21-3360.DC1
Author Manuscript	Author manuscripts have been peer reviewed and accepted for publication but have not yet been edited.

E-mail alerts	Sign up to receive free email-alerts related to this article or journal.
Reprints and Subscriptions	To order reprints of this article or to subscribe to the journal, contact the AACR Publications Department at pubs@aacr.org.
Permissions	To request permission to re-use all or part of this article, use this link http://cancerres.aacrjournals.org/content/early/2021/11/08/0008-5472.CAN-21-3360. Click on "Request Permissions" which will take you to the Copyright Clearance Center's (CCC) Rightslink site.